



Array of symmetric nanohole dimers with high sensitivity for detection of changes in an STT-RAM ultrathin dielectric layer

PARINAZ SADRI-MOSHKENANI,¹ MOHAMMAD WAHIDUZZAMAN KHAN,¹ MD SHAFIQL ISLAM,¹ ILYA KRIVOROTOV,² MIKAEL NILSSON,³ NADER BAGHERZADEH,¹ AND OZDAL BOYRAZ^{1,*} 

¹Department of Electrical Engineering and Computer Science, University of California Irvine, Irvine, California 92697, USA

²Department of Physics and Astronomy, University of California Irvine, Irvine, California 92697, USA

³Department of Chemical and Biomolecular Engineering, University of California Irvine, Irvine, California 92697, USA

*Corresponding author: oboyraz@uci.edu

Received 11 April 2019; revised 17 September 2019; accepted 20 September 2019; posted 24 September 2019 (Doc. ID 364844); published 22 October 2019

A dimer nanohole array is proposed for *in situ* characterization of radiation damages in spin transfer torque random access memory (STT-RAM) multilayer structures. The structure supports a Fano resonance, which is about twice as sensitive to the refractive index changes in the surface layer, compared to the plasmonic mode in single nanohole arrays. A simplified STT-RAM multilayer of air/gold(5 nm)/MgO(10 nm)/gold(60 nm)/quartz substrate is considered as the platform for the dimer nanohole array. Our studies show that regarding the changes in the ultrathin MgO layer, the normalized figure of merit for this structure is up to more than 10 times larger than an array of single nanoholes. Furthermore, an improvement in bulk sensing performance over the array of nanohole heptamers is observed. © 2019 Optical Society of America

<https://doi.org/10.1364/JOSAB.36.003090>

1. INTRODUCTION

In situ measurement of radiation effects requires a high level of sensitivity to the very small changes in material properties due to radiation damage. Optical readout through engineered nanostructures has the potential for high-sensitivity radiation damage detection. For instance, real-time optical measurements of refractive index and absorption profile changes in photonic crystal fibers have been demonstrated in the past [1]. Recently, there is an interest in *in situ* measurement of radiation effects on non-volatile memory cells made of phase changing materials or magnetic tunnel junctions [2,3]. It is important to test their resistance to ionizing radiation, so that we can assure their stability for space applications. Among different types of memory cells, spin transfer torque random access memory (STT-RAM) cells have received a lot of attention because of their high speed, low power, scalability, and high endurance [4–7]. Therefore, our focus here is designing an optical readout scheme for radiation effects in STT-RAM cells. A typical STT-RAM cell is made of multilayer thin films in the form of metal/ferromagnet/dielectric/ferromagnet/metal. In particular, among all the layers of an STT-RAM structure, the dielectric layer, which is usually MgO, is the one that is expected to change the most under an ionizing radiation [8]. Hence, this paper

focuses on detecting changes in optical properties of the dielectric layer. Taking advantage of the metallic layers, we show that it is possible to design plasmonic devices that are sensitive to such changes.

Radiation effects on materials vary significantly. For instance, photodarkening in ytterbium-doped silica glass due to gamma radiation can change the imaginary part of the refractive index several orders of magnitude, depending on the dose of the radiation [9]. Permittivity change of oxides in CMOS is significant enough to alter CMOS operation space applications [10]. There are some materials that show very good radiation tolerance. However, there is no quantified study on the exact magnitude. In particular there is no study available on radiation effects in MgO. Our study shows *in situ* detection of refractive index changes due to radiation effects and sensitivity of photonic detection methods based on information available on SiO₂ parameters. The results presented here can be expanded beyond the defect detection by ionizing radiations.

This paper shows a plasmonic sensor design that can facilitate *in situ* material characterization of radiation damages in STT-RAM structures. In particular, a plasmonic dimer nanohole array that supports a Fano resonance is proposed for high-sensitivity sensing. Since the STT-RAM multilayer includes super thin layers of metal, conventional nanohole array designs

[11] will not work as efficiently for such small thicknesses. The dimer nanohole array presented in this paper provides higher sensitivity at the surface layer, and hence allows better surveillance of the thin dielectric layer, where the most radiation damages occur. Also, since the inter-hole spacing is larger than conventional nanohole cluster array designs [12–14], complexity is manageable. It is worth mentioning that optical spectra of dimer nanohole arrays have been investigated by using polarized and unpolarized light excitation [15–17]. However, high sensitivity of the Fano resonance created by the coupling of surface plasmon polariton (SPP) mode and Wood–Rayleigh anomaly (WA) [18] mode has not been investigated up to date. Here, we show that the coupling between SPP and WA can facilitate a high sensing performance with a figure of merit (FOM) of 40.5 and 486 nm/RIU sensitivity.

To prove the concept, we use a simplified STT-RAM multilayer structure made of metal/dielectric/metal thin films on a dielectric substrate. To make the structure supportive of plasmonic modes, the metal layer sitting on the substrate is set to be an optically thick one. Therefore, the dielectric thin film is placed closer to the surface. From the device point of view, the thickness of the bottom metallic layer has no impact on STT-RAM performance, and it is used as an electrode. We show that the sensitivity to refractive index changes of the dielectric thin film in a multilayer of air/gold(5 nm)/MgO(10 nm)/gold(60 nm)/quartz substrate can be up to twice as large compared to a symmetric nanohole array designed in the same multilayer structure. Furthermore, the sharp Fano resonance results in an FOM improvement of 10.5 times and 1.7 times over different plasmonic resonances in conventional nanohole arrays depending on the excited SPP mode. An estimation of radiation effects is performed based on information available on silica parameters [19], since there is no study available on radiation effects in MgO. According to the sensitivity calculations in this paper and assuming that MgO shows a refractive index change similar to silica after radiation damage (about 3.5%), the radiation-induced wavelength shift is expected to be 0.3 nm.

So far, many works have been done to achieve high sensitivity of plasmonic resonance for sensor applications [20–24]. Some focus on changing the shape of the nanostructures to increase sensitivity. For example, an array of elliptical nanoholes [25] and an array of overlapping dimer nanoholes are introduced [26] to provide larger field enhancement and therefore higher sensitivity by their sharp features in the apices. Furthermore, Fano resonance has been studied as an alternative approach to achieve higher sensitivity. In general, Fano resonance occurs through a coupling between a broadband bright mode and a narrowband dark mode. To make such coupling happen, usually a form of asymmetry is needed. A large number of research efforts have been dedicated to create Fano resonance in arrays of nanoparticles or several combinations of nanoapertures with different aperture shapes [22,27–31]. In particular, clusters of circular nanoholes with heptamer geometry have been proposed as a high-sensitivity plasmonic sensor with improved FOM [12–14]. However, there has been no study of arrays of dimer nanoholes, which is a simpler structure, supporting a Fano resonance.

In what follows, we first provide a comprehensive discussion on the optical behavior of the dimer nanohole array, the origin of the Fano resonance, and how to change the dimensions to make the resonance strong. Next, we investigate the sensing ability of the proposed dimer nanohole array to the changes in refractive index of the ultrathin dielectric layer in the STT-RAM multilayer. We specifically investigate the sensitivity of a multilayer of air/Au(5 nm)/MgO(10 nm)/quartz substrate, derived from STT-RAM structure [6], regarding the changes in the ultrathin dielectric layer (MgO). We also report the bulk sensitivity performance of a dimer nanohole array designed for water as its top layer so that we can compare it with other nanohole array structures.

2. PROPOSED STRUCTURE AND SIMULATION MODEL

The high-sensitivity Fano resonance in a dimer nanohole array can be created through making an asymmetry by moving the nanoholes of a nanohole dimer in a unit cell closer to each other along the dimer axis. Such resonance originates from the excitation of an SPP mode at the top surface (metal/top layer interface), which excites a WA mode at the same interface. An additional form of asymmetry in the structure of a dimer nanohole array that can help strengthen the Fano resonance is the refractive index difference between the top layer and the substrate, similar to the plasmonic nanocube reported in [32]. This is unlike the conventional SPP modes generated in symmetric nanohole arrays, where such refractive index differences can degrade the plasmonic resonance and its sensing performance [33].

To understand the physics of a plasmonic dimer nanohole array, an array of dimer nanoholes in a gold thin film is investigated first. Later in this paper, thin-film MgO and gold layers will be added to estimate the sensitivity to radiation damage. Each unit cell of the dimer nanohole array consists of two nanoholes with the same diameters in a gold thin film on a quartz substrate, covered with an air surrounding layer [Figs. 1(a) and 1(b)]. We used the material data for gold from [34]. Also, the refractive indices for MgO and quartz are set to $n_{\text{MgO}} = 1.73$ and $n_{\text{quartz}} = 1.45$, respectively, which are almost constant over the wavelength range of interest [35,36]. We have used COMSOL Multiphysics 5.4 for all the simulations in this paper. The incident light is normal to the dimer nanohole array, with its E-field polarization along the dimer's axis (y polarized). Because of the symmetry, and to reduce the simulation time, we simulate half of a unit cell [Fig. 1(c)] and use perfect electric conductor (PEC) and perfect magnetic conductor (PMC) boundary conditions on the side walls at xz and yz planes, respectively. Periodic ports are used to illuminate the structure from the substrate side, and perfectly matched layer (PML) boundary conditions are set on the top and bottom of the unit cell behind the ports to absorb the light and to avoid unwanted multiple reflections. It is worth mentioning that the evanescent field at the air side extends to a farther distance from the nanohole dimer in the z direction, compared to the substrate side. Therefore, we put the PML on the air side at a farther distance from the structure.

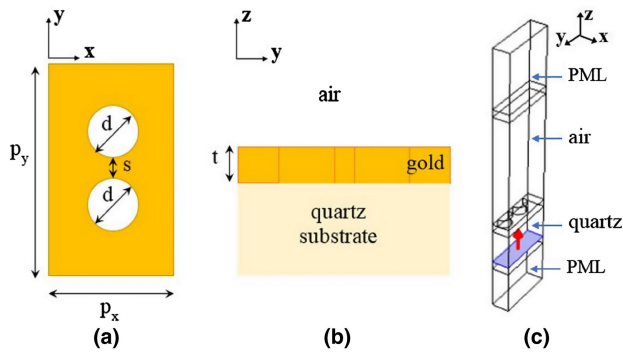


Fig. 1. Unit cell of gold dimer nanohole array: (a) top view, (b) side view, and (c) simulation model in COMSOL Multiphysics 5.4.

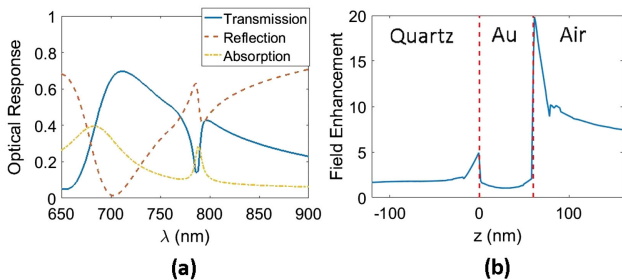


Fig. 2. (a) Optical response of gold dimer nanohole array on quartz substrate ($t = 60$ nm, $d = 250$ nm, $s = 75$ nm, $p_x = 450$ nm, $p_y = 775$ nm). (b) Field enhancement profile of its Fano resonance along the z axis at the location of a major hotspot at the gold/air interface. The dashed lines mark the gold/quartz and gold/air interfaces at $z = 0$ and $z = 60$ nm.

For a nanohole dimer array with dimensions $t = 60$ nm, $d = 250$ nm, $s = 75$ nm, $p_x = 450$ nm, $p_y = 775$ nm, illuminated from the substrate side, by a y -polarized plane wave, the transmission coefficient is plotted in Fig. 2(a). As can be seen, a Fano resonance occurs around 787 nm wavelength. Using the grating formula, and having in mind that WA is the grazing diffraction of light, WA(0,1) mode in a medium with a refractive index of n occurs at a wavelength of $\lambda = np_y$. This means that the WA(0,1) mode at the gold/air interface is theoretically expected to be at $\lambda = 775$ nm, which is very close to the $\lambda = 787$ nm, at which the Fano resonance takes place. It should be noted that the formula used for WA is for PEC, and it would be slightly redshifted for a real metal, as observed here. This is in accordance with the Fano resonance being a result of WA. At the same time, there should be a broad SPP mode happening, creating a large enough transmission coefficient in a range of wavelengths to create the possibility of WA(0,1) at the air side getting efficiently excited. In other words, the excitation of SPP(0,1) at the top layer makes it possible for the WA(0,1) grazing mode to be excited. For the rest of this paper, we focus on the transmission response of the dimer nanohole array. The reason is that it is much simpler in terms of setup alignment, so it will be easier to be measured in practice, compared to reflection and absorption coefficients.

As we mentioned earlier, at the observed Fano resonance, stronger field localization takes place at the air side compared

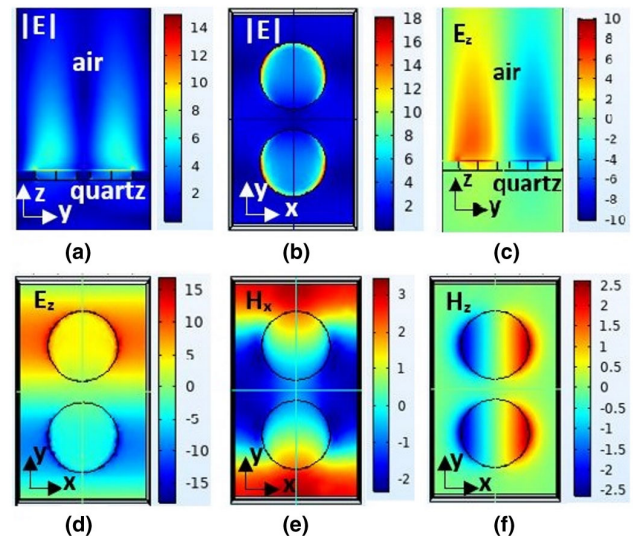


Fig. 3. (a)–(d) E-field and (e), (f) H-field distribution of gold dimer nanohole array on quartz substrate ($t = 60$ nm, $d = 250$ nm, $s = 75$ nm, $p_x = 450$ nm, $p_y = 775$ nm). The xy plane shown in these plots is at $z = 60$ nm (at the gold/air interface).

to the substrate side. This is shown in Fig. 2(b), where the field enhancement is plotted along the z direction at the location of one of the major hotspots at the gold/air interface. This leads us to the expectation of the dimer nanohole array structure being more sensitive to the changes in the top layer, rather than changes in substrate.

To better show the origin of the Fano resonance, the field distributions near a unit cell of the dimer nanohole array are illustrated in Fig. 3 at the Fano resonance wavelength. In the xy plane at the gold/air interface, field localization occurs in the form of four hotspots [Figs. 3(b) and 3(f)]. It is clear from the plots in the yz plane that the field is localized mainly at the gold/air interface. Also, the xy plane plots for E_z and H_x show the wave propagation along the y axis, which is the characteristic of SPP(0,1) and WA(0,1) modes. Although the defects we try to sense are not sensitive to the magnetic field, magnetic field distributions are shown in Figs. 3(e) and 3(f) to provide a better sense of the excited resonance mode.

A. Effect of Changing Dimensions

Changing the dimensions affects the strength of the aforementioned Fano resonance in metal dimer nanohole arrays. Again, quartz is considered here as the substrate, gold as the plasmonic metal, and air as the top layer. The simulation results for the changes in the width and magnitude of the Fano resonance as well as the maximum field enhancement on the air side (FE_{max}) at the Fano resonance will be discussed. In all the cases, the nanoholes in the nanohole dimer are set to have equal diameters (symmetric nanohole dimer).

The effect of changing p_y on the transmission spectrum and the maximum field enhancement on the air side is shown in Fig. 4. Increasing p_y increases the Fano resonance wavelength proportionally, while for each p_y , the resonance wavelength is close to the value of p_y . This supports the fact that the Fano resonance is caused by the WA(0,1) mode propagating in the

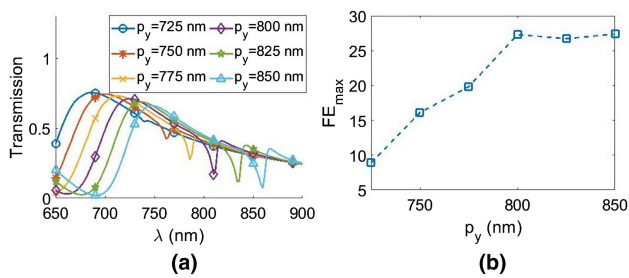


Fig. 4. Effect of changing p_y on (a) transmission spectrum and (b) maximum field enhancement ($p_x = 450$ nm, $s = 100$ nm, $d = 250$ nm, $t = 60$ nm).

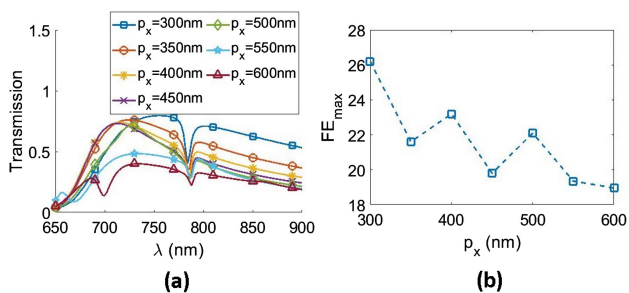


Fig. 5. Effect of changing p_x on (a) transmission spectrum and (b) maximum field enhancement ($p_y = 775$ nm, $s = 100$ nm, $d = 250$ nm, $t = 60$ nm).

y direction. Also, as p_y increases, the Fano resonance gets stronger (deeper resonance feature in transmission spectrum and larger FE_{max}). This is because the larger the p_y , the more asymmetry is created in the structure in the y direction, since the difference between the inter-hole spacing between the nearest nanoholes in two adjacent unit cells and the one between the nanoholes inside a unit cell becomes larger. Another thing to notice is that increasing p_y increases the peak wavelength of the transmission spectrum, which is in agreement with the large broad transmission being a result of excitation of SPP(0,1) mode.

On the other hand, changing the period in the x direction (p_x) does not change the Fano resonance wavelength [Fig. 5(a)]. The reason is that the WA(0,1) mode is the decision maker for the Fano resonance wavelength, and it propagates along the y direction, which has nothing to do with the period in the x direction. However, increasing p_x reduces the depth of the Fano resonance at the resonance wavelength. This is expected, since a larger p_x decreases the ratio of nanohole-to-metal area in the dimer nanohole array, so there is less light coupled to the SPP mode and therefore the WA mode at the gold/air interface. Also in Fig. 5(b), FE_{max} is plotted at the Fano resonance for different values of p_x . It shows an overall trend of FE_{max} decreasing by increasing p_x , which is in accordance with the Fano resonance getting weaker because of less coupling to the WA mode. There are some irregularities in the overall falling trend though. This is because of the sampling error created by a relatively large wavelength step chosen in the simulations, and it is kept that way for the sake of consistency with the rest of the results in this

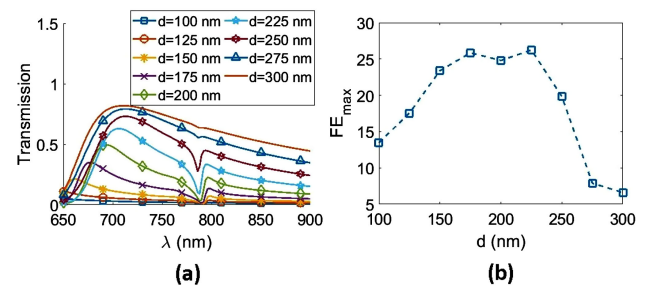


Fig. 6. Effect of changing the nanohole diameter on (a) transmission spectrum and (b) maximum field enhancement ($p_x = 450$ nm, $p_y = 775$ nm, $s = 100$ nm, $t = 60$ nm).

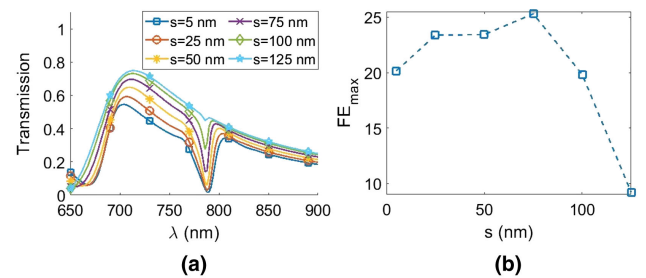


Fig. 7. Effect of changing the inter-hole spacing on (a) transmission spectrum and (b) maximum field enhancement ($p_x = 450$ nm, $p_y = 775$ nm, $d = 250$ nm, $t = 60$ nm).

paper. Smaller wavelength steps show a constantly falling trend for FE_{max} as p_x increases.

It is worth mentioning that in Fig. 5(a), the dip at $\lambda = 700$ nm for the case of $p_x = 600$ nm is because of the WA(1,1) mode at the gold/quartz interface, which is theoretically expected to be at $\lambda = 688$ nm. The same thing is true for $p_x = 550$ nm at $\lambda = 670$ nm, which is theoretically expected to occur at $\lambda = 650$ nm.

The nanohole diameter and the inter-hole spacing have a correlated effect on the strength of the Fano resonance. In other words, depending on the nanohole diameter, there is a specific value of inter-hole spacing that results in the strongest Fano resonance. This is shown in Figs. 6 and 7. For example, from these figures, one can observe that for a dimer nanohole array with x and y periods and thicknesses of $p_x = 450$ nm, $p_y = 775$ nm, and $t = 60$ nm, two cases of $d = 225$ nm, $s = 100$ nm, and $d = 250$ nm, $s = 75$ nm are the best choices in terms of providing a sharp Fano resonance as well as a large FE_{max} .

According to further studies we did, which are not shown in this paper, if we keep p_y constant, for a larger nanohole diameter, there will be a need for a smaller inter-hole spacing to achieve a strong Fano resonance. For example, keeping $p_y = 775$ nm, the Fano resonance for $d = 300$ nm, $s = 5$ nm is almost as strong as the one for $d = 250$ nm, $s = 75$ nm. This is because of the fact that p_y is fixed for all cases, so a larger nanohole diameter needs a smaller s to create a large enough asymmetry between s and the inter-hole spacing between a nanohole and its adjacent nanohole in the next unit cell. Also,

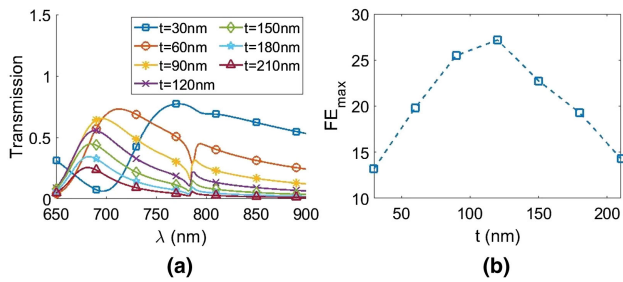


Fig. 8. Effect of changing the gold thickness on (a) transmission spectrum and (b) maximum field enhancement ($p_x = 450$ nm, $p_y = 775$ nm, $d = 250$ nm, $s = 100$ nm).

for a smaller nanohole diameter, the transmission for the broadband SPP(0,1) mode decreases, which leads to a weaker Fano resonance because of less coupling to the SPP mode and thus to the WA mode.

After all, the thickness of the gold layer can affect the strength of the Fano resonance. It can be seen in Fig. 8 that if the gold layer gets so thin that the thickness is so close to the skin depth of the gold, the Fano resonance broadens and gets weaker, which is because the gold layer is not functioning as a good metal in that case. On the other hand, for the thickness of 150 nm or more, the Fano resonance starts to become less deep, and the FE_{\max} gradually decreases. The reason is that the coupling to the SPP mode and therefore to the WA mode decreases by increasing the gold thickness. The maximum thickness for which the Fano resonance can stay relatively strong depends on the nanohole diameter, since increasing the nanohole diameter can help increase the coupling to the SPP and WA modes. However, there is a limit because a larger nanohole diameter needs a smaller inter-hole spacing to get a strong Fano resonance, as discussed earlier in this section.

3. SENSITIVITY AND FIGURE OF MERIT

As mentioned earlier, one of the main applications of metallic nanohole arrays is sensing the refractive index of the dielectric material close to the metal layer. The sensing capability is usually compared by two parameters. The first parameter is sensitivity, which is the shift in the resonance wavelength divided by the change in the refractive index of the dielectric material. The other parameter defined as a measure for sensing is FOM, which is sensitivity divided by linewidth.

As stated before, we expect the proposed dimer nanohole array to have better sensing performance regarding a refractive index change close to the gold/air interface. In this section, we first focus on sensing the changes in the ultrathin dielectric layer (MgO) in a dimer nanohole array formed in a multilayer platform as a simplified version of STT-RAM structure, with the purpose of detecting the effect of ionizing irradiation on STT-RAM cells. After that, we provide the results for bulk sensing for a quartz/gold(60 nm)/air dimer nanohole array. In both cases, the nanoholes are assumed to extend thoroughly in the gold layers and the MgO layer. We report the values of sensitivity and FOM, and compare them to the case of a symmetric nanohole array we designed and heptamer nanohole array reported elsewhere.

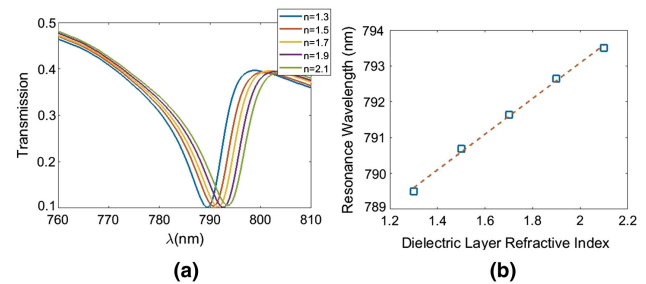


Fig. 9. Sensitivity evaluation regarding the ultrathin dielectric layer for the STT-RAM multilayer dimer nanohole array ($p_x = 450$ nm, $p_y = 775$ nm, $d = 250$ nm, $s = 75$ nm). (a) Transmission spectra for different refractive indices of the ultrathin dielectric layer. (b) Fano resonance wavelength versus refractive index of the ultrathin film dielectric layer.

A. Sensitivity to Ultrathin Dielectric Layer

To evaluate the sensing capability of the proposed dimer nanohole array regarding the ultrathin MgO layer in the STT-RAM structure, we investigate a dimer nanohole array in a quartz/gold(60 nm)/MgO(10 nm)/gold(5 nm)/air multilayer. The dimensions of the dimer nanohole array considered for this purpose are $p_x = 450$ nm, $p_y = 775$ nm, $d = 250$ nm, $s = 75$ nm. The sensitivity is evaluated by changing the refractive index of the MgO layer from $n = 1.3$ to $n = 2.1$ by increments of 0.2 (Fig. 9). Based on these results, the Fano resonance shows a linewidth of 11 nm. There is no established dose test for MgO, so here we take silica as base, which shows a refractive index change of ~ 0.05 (about 3.5%) under ion beam radiation using Br ions with a dose level of about 46 krad as presented in [19]. Considering the same percentage of refractive index change for MgO, the radiation-induced wavelength shift for the designed dimer nanohole array structure is expected to be 0.3 nm. One should keep in mind that the refractive index change would be different for a different ion type and energy of the ion beam, as shown in [37].

To make a comparison with a conventional nanohole array [11], we have designed two nanohole arrays in the same multilayer platform, with dimensions $d = 200$ nm, $p = 460$ nm (NHA-1), and $d = 400$ nm, $p = 750$ nm (NHA-2), designed to show field localization at the top layer, by excitation of first-order SPP mode at the surface layer through coupling with the SPP mode at the gold/quartz interface, or directly through the grating effect, respectively. We have included the results of both in Fig. 10.

Using these results and normalizing them to the area of the MgO layer per unit cell area in the xy plane ($1 - 2A_{\text{nanohole}}/A_{\text{unitcell}}$) to have a fair comparison, the normalized sensitivity of NHA-1 and NHA-2 are found to be about 2 and 1.3 times less than the sensitivity of the designed dimer nanohole array, respectively. Furthermore, their calculated normalized FOM values are about 10.5 and 1.7 times less compared to the designed dimer nanohole arrays. NHA-1 has a larger linewidth, and its smaller sensitivity is because the field is more localized at the substrate side in that case due to indirect excitation of the SPP mode at the air side. On the other hand, NHA-2 shows better sensing performance, since the SPP mode at the air

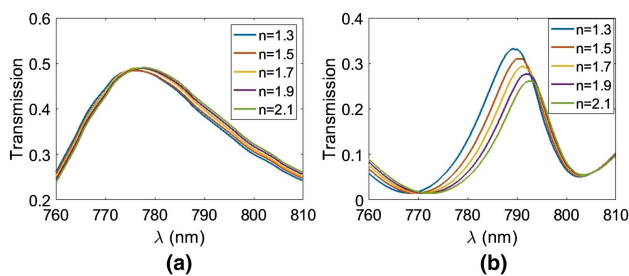


Fig. 10. Sensitivity evaluation regarding the ultrathin dielectric layer for the designed STT-RAM multilayer symmetric nanohole arrays: (a) NHA-1 with dimensions $p = 460$ nm, $d = 200$ nm and (b) NHA-2 with dimensions $p = 750$ nm, $d = 400$ nm.

side is directly excited. However, its sensing performance is 70% less than the proposed dimer nanohole array.

B. Bulk Sensitivity

For bulk sensitivity, we set the top layer as water, because it is the most common case for bulk material sensing in the literature. Since the top layer is changed to water, there is a need for changing the dimensions to achieve the Fano resonance in the same wavelength range. If we keep $p_y = 775$ nm, because the refractive index of the top layer here ($n = 1.33$) is larger than in the previous cases, the Fano resonance created by the excitation of WA(0,1) mode at the gold/top layer interface happens at a longer wavelength, which is outside our wavelength range of study. Decreasing p_y moves the resonance wavelength back to the desired wavelength range. Tuning the diameter and inter-hole spacing to get a sharp resonance, we chose the nanohole dimensions as $p_x = 450$ nm, $p_y = 520$ nm, $d = 200$ nm, $s = 20$ nm, $t = 60$ nm.

The simulation results for bulk sensitivity evaluation are provided in Fig. 11. Two Fano resonances are observed, created by the coupling of the SPP(0,1) mode at the gold/water interface and a WA mode at the gold/water interface or at the gold/quartz interface. The one with the larger resonance wavelength ($\lambda = 790$ nm for $n = 1.33$) is created by excitation of WA(0,1) mode at the gold/quartz interface, and the resonance with smaller wavelength ($\lambda = 723$ nm for $n = 1.33$) occurs because of the excitation of WA(0,1) mode at the gold/water interface. This is why the Fano resonance with the smaller resonance wavelength is much more sensitive to the refractive index changes in the top layer. The two Fano resonances here in this design are very close to each other, which was not observed in previous designs in this paper. The reason is that water is considered as the top layer here for bulk sensing, the refractive index of which is closer to the one for substrate. Therefore, the WA modes show up closer to each other in the spectral response.

According to the simulation results, the calculated bulk sensitivity of the dimer nanohole array is 486 nm/RIU. Having a 12 nm linewidth, the calculated FOM for the bulk sensitivity is 40.5, which is larger than the highest FOM reported in [14] for a heptamer nanohole array (FOM = 23.8). It is worth mentioning that using a dimer nanohole array for sensing purposes relaxes the fabrication complexity, compared to larger clusters

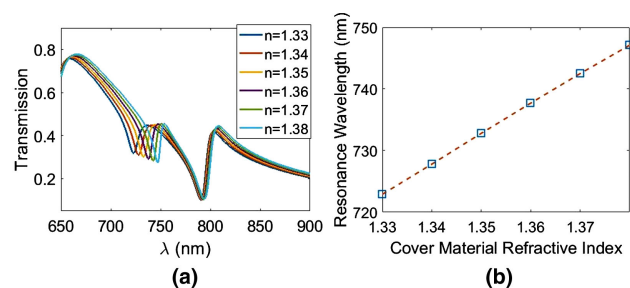


Fig. 11. Bulk sensitivity evaluation for gold dimer nanohole array on a quartz substrate with water as top layer ($p_x = 450$ nm, $p_y = 520$ nm, $d = 200$ nm, $s = 20$ nm, $t = 60$ nm). (a) Transmission spectra for different refractive indices of the top layer. (b) Fano resonance wavelength versus refractive index of the top layer for the Fano resonance with shorter resonance wavelength.

of nanoholes, since the inter-hole spacing can be set to a larger value, increasing the minimum feature size.

To compare with a conventional symmetric nanohole array, there are many papers reporting its sensing performance [38–44], among which an FOM of 40 is the highest, reported in [43]. Although the design provided here for bulk sensing of a dimer nanohole array is not optimized to provide the highest possible sensitivity, it shows a slightly larger figure of merit compared to the one reported for a symmetric nanohole array. Furthermore, the design reported in [43] is based on an etched substrate, which provides more overlap of the surrounding material with the plasmonic field profile, resulting in an increase in sensitivity. A better comparison would be with [42], where a similar substrate is used, and reports FOM of 23.3.

There are also arrays of different nanostructure shapes based on SPP sensing that one can compare with, such as a nanoslit array [45] (FOM: 33.9), elliptic nanohole array [46] (FOM~16.5), and array of overlapped double holes [26] (FOM~16.3). Having the reported FOM values for those structures, one can observe that our design shows a better sensing performance.

4. SUMMARY AND CONCLUSION

We propose a dimer nanohole array in a plasmonic metal film, which has a Fano resonance highly sensitive to the refractive index of the top layer, or any thin-film layer placed on top. We provide the simulation results for two cases of ultrathin film sensing, which is specifically evaluated for a simplified STT-RAM multilayer, with an incentive of sensing the irradiation effects. We show that the dimer nanohole array has 10.5 times and 1.7 times better sensing performance than a conventional symmetric nanohole array depending on the type of plasmonic resonance in the symmetric nanohole array. Also, we provide the results for bulk material sensing with the dimer nanohole array, a sensitivity of 486 nm/RIU with FOM of 40.5, which are both larger than the ones reported previously for a symmetric nanohole array and heptamer nanohole array.

Funding. Defense Threat Reduction Agency (HDTRA1-16-1-0025).

REFERENCES

- S. Girard, J. Baggio, and J.-L. Leray, "Radiation-induced effects in a new class of optical waveguides: the air-guiding photonic crystal fibers," *IEEE Trans. Nucl. Sci.* **52**, 2683–2688 (2005).
- P. Sadri-Moshkenani, M. W. Khan, Q. Zhao, I. Krivorotov, M. Nilsson, N. Bagherzadeh, and O. Boyraz, "Plasmonic detection of possible defects in multilayer nanohole array consisting of essential materials in simplified STT-RAM cell," *Proc. SPIE* **10346**, 1034639 (2017).
- P. Sadri-Moshkenani, M. W. Khan, M. S. Islam, I. Krivorotov, M. Nilsson, N. Bagherzadeh, and O. Boyraz, "Array of symmetric nanohole dimers for STT-RAM ultrathin layer sensing," in *Conference on Lasers and Electro-Optics (CLEO) (2019)*, paper JW2A.60.
- P. Zhou, B. Zhao, J. Yang, and Y. Zhang, "Energy reduction for STT-RAM using early write termination," in *Proceedings of the 2009 International Conference on Computer-Aided Design (ACM, 2009)*, pp. 264–268.
- S. Chung, K.-M. Rho, S.-D. Kim, H.-J. Suh, D.-J. Kim, H.-J. Kim, S.-H. Lee, J.-H. Park, H.-M. Hwang, S.-M. Hwang, and J. Y. Lee, "Fully integrated 54nm STT-RAM with the smallest bit cell dimension for high density memory application," in *Electron Devices Meeting (EDM), 2010 IEEE International (IEEE, 2010)*, pp. 12–17.
- K. Wang, J. Alzate, and P. K. Amiri, "Low-power non-volatile spintronic memory: STT-RAM and beyond," *J. Phys. D* **46**, 074003 (2013).
- M.-T. Chang, P. Rosenfeld, S.-L. Lu, and B. Jacob, "Technology comparison for large last-level caches (l3 cs): Low-leakage SRAM, low write-energy STT-RAM, and refresh-optimized EDRAM," in *IEEE 19th International Symposium on High Performance Computer Architecture (HPCA2013) (IEEE, 2013)*, pp. 143–154.
- K. Galloway and R. Schrimpf, "MOS device degradation due to total dose ionizing radiation in the natural space environment: a review," *Microelectron. J.* **21**, 67–81 (1990).
- T. Arai, K. Ichii, S. Tanigawa, and M. Fujimaki, "Gamma-radiation-induced photodarkening in ytterbium-doped silica glasses," *Proc. SPIE* **7914**, 79140K (2011).
- J. R. Schwank, M. R. Shaneyfelt, D. M. Fleetwood, J. A. Felix, P. E. Dodd, P. Paillet, and V. Ferlet-Cavrois, "Radiation effects in MOS oxides," *IEEE Trans. Nucl. Sci.* **55**, 1833–1853 (2008).
- L. Martin-Moreno, F. Garcia-Vidal, H. Lezec, K. Pellerin, T. Thio, J. Pendry, and T. Ebbesen, "Theory of extraordinary optical transmission through subwavelength hole arrays," *Phys. Rev. Lett.* **86**, 1114 (2001).
- Y. Zhan, D. Y. Lei, X. Li, and S. A. Maier, "Plasmonic Fano resonances in nanohole quadruplers for ultra-sensitive refractive index sensing," *Nanoscale* **6**, 4705–4715 (2014).
- J. He, P. Ding, J. Wang, C. Fan, and E. Liang, "Double Fano-type resonances in heptamer-hole array transmission spectra with high refractive index sensing," *J. Mod. Opt.* **62**, 1241–1247 (2015).
- A. Hajejbifard and P. Berini, "Fano resonances in plasmonic heptamer nano-hole arrays," *Opt. Express* **25**, 18566–18580 (2017).
- R. Gordon, M. Hughes, B. Leathem, K. Kavanagh, and A. Brolo, "Basis and lattice polarization mechanisms for light transmission through nanohole arrays in a metal film," *Nano Lett.* **5**, 1243–1246 (2005).
- W. Yue, Z. Wang, Y. Yang, J. Li, Y. Wu, L. Chen, B. Ooi, X. Wang, and X.-X. Zhang, "Enhanced extraordinary optical transmission (EOT) through arrays of bridged nanohole pairs and their sensing applications," *Nanoscale* **6**, 7917–7923 (2014).
- Y. Zhang, M. Han, and C.-P. Huang, "Plasmon coupling in circular-hole dimers: from separation-to touching-coupling regimes," *J. Appl. Phys.* **112**, 013113 (2012).
- D. Maystre, "Theory of Wood's anomalies," in *Plasmonics* (Springer, 2012), pp. 39–83.
- O. Peña-Rodríguez, J. Manzano-Santamaría, J. Olivares, A. Rivera, and F. Agulló-López, "Refractive index changes in amorphous sio2 (silica) by swift ion irradiation," *Nucl. Instrum. Methods Phys. Res., Sect. B* **277**, 126–130 (2012).
- S. Liu, Z. Zhang, and Q. Wang, "High sensitivity and large field enhancement of symmetry broken au nanorings: effect of multipolar plasmon resonance and propagation," *Opt. Express* **17**, 2906–2917 (2009).
- A. Kabashin, P. Evans, S. Pastkovsky, W. Hendren, G. Wurtz, R. Atkinson, R. Pollard, V. Podolskiy, and A. Zayats, "Plasmonic nanorod metamaterials for biosensing," *Nat. Mater.* **8**, 867 (2009).
- N. Liu, T. Weiss, M. Mesch, L. Langguth, U. Eigenthaler, M. Hirscher, C. Sonnichsen, and H. Giessen, "Planar metamaterial analogue of electromagnetically induced transparency for plasmonic sensing," *Nano Lett.* **10**, 1103–1107 (2009).
- C.-Y. Tsai, S.-P. Lu, J.-W. Lin, and P.-T. Lee, "High sensitivity plasmonic index sensor using slablike gold nanoring arrays," *Appl. Phys. Lett.* **98**, 153108 (2011).
- A. E. Cetin, A. F. Coskun, B. C. Galarreta, M. Huang, D. Herman, A. Ozcan, and H. Altug, "Handheld high-throughput plasmonic biosensor using computational on-chip imaging," *Light Sci. Appl.* **3**, e122 (2014).
- G. A. C. Tellez, R. N. Tait, P. Berini, and R. Gordon, "Atomically flat symmetric elliptical nanohole arrays in a gold film for ultrasensitive refractive index sensing," *Lab Chip* **13**, 2541–2546 (2013).
- A. Lesuffleur, H. Im, N. C. Lindquist, and S.-H. Oh, "Periodic nanohole arrays with shape-enhanced plasmon resonance as real-time biosensors," *Appl. Phys. Lett.* **90**, 243110 (2007).
- K. Bao, N. A. Mirin, and P. Nordlander, "Fano resonances in planar silver nanosphere clusters," *Appl. Phys. A* **100**, 333–339 (2010).
- B. Luk'yanchuk, N. I. Zheludev, S. A. Maier, N. J. Halas, P. Nordlander, H. Giessen, and C. T. Chong, "The Fano resonance in plasmonic nanostructures and metamaterials," *Nat. Mater.* **9**, 707 (2010).
- J. Chen, P. Wang, C. Chen, Y. Lu, H. Ming, and Q. Zhan, "Plasmonic EIT-like switching in bright-dark-bright plasmon resonators," *Opt. Express* **19**, 5970–5978 (2011).
- T. K. Nguyen, T. D. Le, P. T. Dang, and K. Q. Le, "Asymmetrically engineered metallic nanodisk clusters for plasmonic Fano resonance generation," *J. Opt. Soc. Am. B* **34**, 668–672 (2017).
- J. Chen, Z. Li, S. Yue, J. Xiao, and Q. Gong, "Plasmon-induced transparency in asymmetric t-shape single slit," *Nano Lett.* **12**, 2494–2498 (2012).
- S. Zhang, K. Bao, N. J. Halas, H. Xu, and P. Nordlander, "Substrate-induced Fano resonances of a plasmonic nanocube: a route to increased-sensitivity localized surface plasmon resonance sensors revealed," *Nano Lett.* **11**, 1657–1663 (2011).
- M. Najiminaini, F. Vasefi, B. Kaminska, and J. J. Carson, "Nano-hole array structure with improved surface plasmon energy matching characteristics," *Appl. Phys. Lett.* **100**, 043105 (2012).
- P. B. Johnson and R.-W. Christy, "Optical constants of the noble metals," *Phys. Rev. B* **6**, 4370–4379 (1972).
- R. E. Stephens and I. H. Malitson, "Index of refraction of magnesium oxide," *J. Res. Natl. Bur. Stand.* **49**, 249–252 (1952).
- I. Malitson, "Interspecimen comparison of the refractive index of fused silica," *J. Opt. Soc. Am.* **55**, 1205–1209 (1965).
- J. Manzano, J. Olivares, F. Agulló-López, M. Crespillo, A. Moroño, and E. Hodgson, "Optical waveguides obtained by swift-ion irradiation on silica (a-sio2)," *Nucl. Instrum. Methods Phys. Res., Sect. B* **268**, 3147–3150 (2010).
- J. W. de Menezes, A. Thesing, C. Valsecchi, L. E. Armas, and A. G. Brolo, "Improving the performance of gold nanohole array biosensors by controlling the optical collimation conditions," *Appl. Opt.* **54**, 6502–6507 (2015).
- A. De Leebeek, L. S. Kumar, V. De Lange, D. Sinton, R. Gordon, and A. G. Brolo, "On-chip surface-based detection with nanohole arrays," *Anal. Chem.* **79**, 4094–4100 (2007).
- J. Ferreira, M. J. Santos, M. M. Rahman, A. G. Brolo, R. Gordon, D. Sinton, and E. M. Girotto, "Attomolar protein detection using in-hole surface plasmon resonance," *J. Am. Chem. Soc.* **131**, 436–437 (2008).
- J. W. Menezes, J. Ferreira, M. J. Santos, L. Cescato, and A. G. Brolo, "Large-area fabrication of periodic arrays of nanoholes in metal films and their application in biosensing and plasmonic-enhanced photovoltaics," *Adv. Funct. Mater.* **20**, 3918–3924 (2010).
- J. Henzie, M. H. Lee, and T. W. Odom, "Multiscale patterning of plasmonic metamaterials," *Nat. Nanotechnol.* **2**, 549 (2007).
- A. A. Yanik, M. Huang, O. Kamohara, A. Artar, T. W. Geisbert, J. H. Connor, and H. Altug, "An optofluidic nanoplasmonic biosensor for

- direct detection of live viruses from biological media," *Nano Lett.* **10**, 4962–4969 (2010).
44. A.-P. Blanchard-Dionne and M. Meunier, "Sensing with periodic nanohole arrays," *Adv. Opt. Photon.* **9**, 891–940 (2017).
45. K.-L. Lee, P.-W. Chen, S.-H. Wu, J.-B. Huang, S.-Y. Yang, and P.-K. Wei, "Enhancing surface plasmon detection using template-stripped gold nanoslit arrays on plastic films," *ACS Nano* **6**, 2931–2939 (2012).
46. J. Yuan, Y. Xie, Z. Geng, C. Wang, H. Chen, Q. Kan, and H. Chen, "Enhanced sensitivity of gold elliptic nanohole array biosensor with the surface plasmon polaritons coupling," *Opt. Mater. Express* **5**, 818–826 (2015).